[PS]Quantitative Prediction of Three-Dimensional Facies Architecture and Heterogeneity in Meandering Fluvial Successions*

Na Yan[1], Nigel P. Mountney[1], Luca Colombera[1]

Search and Discovery Article #51497 (2018)**
Posted July 16, 2018

*Adapted from poster presentation at AAPG ACE 2018 Annual Convention & Exhibition, Salt Lake City, Utah, May 20-23, 2018

[1]School of Earth and Environment, University of Leeds, Leeds, United Kingdom. (N.Yan@leeds.ac.uk)

Abstract

Fluvial meander bends undertake expansion, translation, rotation and combinations thereof as they evolve. However, relationships between the migratory behavior of a river, the geometry of accumulated sedimentary bodies (e.g., point bars, counter-point bars) that arise from channel migration, and the resultant internal lithofacies distribution within these bodies remain relatively poorly understood. To explore the relationship between fluvial channel evolution and resultant accumulated stratigraphic architecture, a forward numerical stratigraphic model – the *Point-Bar Sedimentary Architecture Numerical Deduction (PB-SAND)* – has been developed that uses a combined geometric-stochastic approach. The model is applied to predict types of lithological heterogeneity and sandbody connectivity in fluvial successions for a variety of meandering river types.

The modeling approach is constrained by quantified sedimentological data from real-world case-study examples stored in a relational database, the Fluvial Architecture Knowledge Transfer System (FAKTS). The model has the following capabilities: 1) to replicate bar-growth trajectories and sedimentary structures of meandering systems based on real-world data of sedimentary architecture derived from modern rivers and ancient successions that serve as geologic analogs; 2) to examine the sensitivity of intrinsic system behavior to different allogenic controls operating at varying spatial and temporal scales, such as point-bar elements in humid coastal plain vs. dryland fluvial fan settings; 3) to quantify the heterogeneity and compartmentalization arising from intra-bar mud drapes; 4) to predict the sedimentary architecture of meander belts arising from repeated migration and avulsion of river reaches; 5) to predict fluvial sandbody stacking patterns, for example in response to coeval rift basin development.

The grid-free, 3D model provides linkage between local outcrop measurements and large-scale evolutionary behavior, and allows quantitative assessments of possible scenarios depicted in traditional qualitative facies models. Output from PB-SAND can be employed to condition reservoir models at different spatial scales, notably by creating training images for constraining models built through techniques based on Multi-Point Statistics. More realistic architectural geometries and spatial distributions of facies associations markedly enhance conventional reservoir models, thereby improving fluid-flow simulations.

References Cited

Alexander, J., and M.R. Leeder, 1987, Active tectonic control on alluvial architecture, *in* F. G. Ethridge, R.M. Flores, and M.D. Harvey, editors, Recent Developments in Fluvial Sedimentology, SEPM Special Publication 39, p. 243-252.

Colombera, L., N.P. Mountney, and W.D. McCaffrey, 2013, A quantitative approach to fluvial facies models: Methods and example results: Sedimentology, 60, 1526-1558.

Colombera, L., N. Yan, T. McCormick-Cox, and N.P. Mountney, 2018, Seismic-driven geocellular modeling of fluvial meander-belt reservoirs using a rule-based method: Marine and Petroleum Geology.

Donselaar, M.E., and I. Overeem, 2008, Connectivity of fluvial point-bar deposits: An example from the Miocene Huesca fluvial fan, Ebro Basin, Spain: AAPG Bulletin, 92/9, p. 1109-1129.

Ghazi, S., and N.P. Mountney, 2009, Facies and architectural element analysis of a meandering fluvial succession: The Permian Warchha Sandstone, Salt Range, Pakistan. Sedimentary Geology, v. 221/1-4,p. 99-126.

Ghinassi, M., and A. Ielpi, 2015, Stratal architecture and morphodynamics of downstream-migrating fluvial point bars (Jurassic Scalby Formation, U.K.): Journal of Sedimentary Research, v. 85/9, p. 1123-1137.

Ghinassi, M., A. Ielpi, M. Aldinucci, and F. Fustic, 2016, Downstream-migrating fluvial point bars in the rock record. Sedimentary Geology, v. 334, p. 66-96.

Hartley, A.J., A. Owen, A. Swan, G.S. Weissmann, B.I. Holzweber, J. Howell, G. Nichols, and L. Scuderi, 2015, Recognition and importance of amalgamated sandy meander belts in the continental rock record: Geology, v. 43/8, p. 679-682.

Maynard, K., and I. Murray, 2003, One million years from the Upper Arang Formation, West Natuna Basin: Implications for reservoir distribution and facies variation in fluvial deltaic deposits: Proceedings ofAnnual Convention, Indonesian Petroleum Association, v. 29, p.. 267-276.

Reijenstein, H.M., H.W. Posamentier, and J.P. Bhattacharya, 2011, Seismic geomorphology and high-resolution seismic stratigraphy of inner-shelf fluvial, estuarine, deltaic, and marine sequences, Gulf of Thailand: AAPG Bulletin, v. 95/11, p. 1959-1990.

Smith, D.G., S.M. Hubbard, D.A. Leckie, and M. Fustic, 2009, Counter point bar deposits: lithofacies and reservoir significance in the meandering modern Peace River and ancient McMurray Formation, Alberta, Canada: Sedimentology, v.56, p. 1655-1669.

Smith, R.M.H., 1987, Morphology and depositional history of exhumed Permian point bars in the southwestern Karoo, South Africa: Journal of Sedimentary Research, v. 57/1, p. 19-29.

Smith, D.G., S.M. Hubbard, J.R. Lavigne, D.A. Leckie, and M. Fustic, 2011, Stratigraphy of counter-point-bar and eddy-accretion deposits in low-energy meander belts of the Peace-Athabasca Delta, Northeast Alberta, Canada, *in* S.K. Davidson, S. Leleu, and C.P. North, editors, From River to Rock Record: The Preservation of Fluvial Sediments and Their Subsequent Interpretation: Society for Sedimentary Geology Special Publication, Tulsa, p. 143-152.

Trendell, A.M., S.C. Atchley, and L.C. Nordt, 2013, Facies analysis of a probable large-fluvial-fan depositional system: The Upper Triassic Chinle Formation at Petrified Forest National Park, Arizona, USA: Journal of Sedimentary Research, v. 83/10, p. 873-895.

Wu, C., J. P. Bhattacharya, and M.S. Ullah, 2015, Paleohydrology and 3D facies architecture of ancient point bars, Ferron Sandstone, Notom Delta, south-central Utah, USA: Journal of Sedimentary Research, v. 85/4, p. 399-418.

Yan, N., N.P. Mountney, L., Colombera, and R.M. Dorrell, 2017, A 3D forward stratigraphic model of fluvial meander-bend evolution for prediction of point-bar lithofacies architecture. Computers & Geosciences, v. 105, p. 65-80.

Yan, N., N.P. Mountney, L., Colombera, and R.M. Dorrell, 2018, Fluvial point-bar architecture and facies heterogeneity, and their influence on intra-bar static connectivity in humid coastal-plain and dryland fan systems: Special Publications of the International Association of Sedimentologists, 48.

Quantitative Prediction of Three-Dimensional Facies Architecture and Heterogeneity in Meandering Fluvial Successions

Na Yan, Nigel P. Mountney, Luca Colombera

Fluvial & Eolian Research Group, University of Leeds, UK

Abstract

Fluvial meander bends undertake expansion, translation, rotation and combinations thereof as they evolve. However, relationships between the migratory behavior of a river, the geometry of accumulated sedimentary bodies (e.g., point bars, counter-point bars) that arise from channel migration, and the resultant internal lithofacies distribution within these bodies remain relatively poorly understood. To explore the relationship between fluvial channel evolution and resultant accumulated stratigraphic architecture, a forward numerical stratigraphic model – the Point-Bar Sedimentary Architecture Numerical Deduction (PB-SAND) – has been developed that uses a combined geometric-stochastic approach. The model is applied to predict types of lithological heterogeneity and sandbody connectivity in fluvial successions for a variety of meandering river types.

The modeling approach is constrained by quantified sedimentological data from real-world case-study examples stored in a relational database, the Fluvial Architecture Knowledge Transfer System (FAKTS). The model has the following capabilities: 1) to replicate bar-growth trajectories and sedimentary structures of meandering systems based on real-world data of sedimentary architecture derived from modern rivers and ancient successions that serve as geologic analogs; 2) to examine the sensitivity of intrinsic system behavior to different allogenic controls operating at varying spatial and temporal scales, such as point-bar elements in humid coastal plain vs. dryland fluvial fan settings; 3) to quantify the heterogeneity and compartmentalization arising from intra-bar mud drapes; 4) to predict the sedimentary architecture of meander belts arising from repeated migration and avulsion of river reaches; 5) to predict fluvial sandbody stacking patterns, for example in response to coeval rift basin development.

The grid-free, 3D model provides linkage between local outcrop measurements and large-scale evolutionary behavior, and allows quantitative assessments of possible scenarios depicted in traditional qualitative facies models. Output from PB-SAND can be employed to condition reservoir models at different spatial scales, notably by creating training images for constraining models built through techniques based on Multi-Point Statistics. More realistic architectural geometries and spatial distributions of facies associations markedly enhance conventional reservoir models, thereby improving fluid-flow simulations.

Introduction and Background

Basic meander-bend transformations have been well-recognised: expansion, translation, rotation, and combinations thereof. The relationship between point-bar geometry, migration, and facies distribution (in both plan views and vertical successions), however, remains inadequately understood, principally because of the limited availability of field data in the form of 2D outcrop sections in the rock record, and partially because of difficulty in reconstructing complex evolutionary history and internal architecture of meander bends. Stratigraphic successions of fluvial point-bar elements are typically characterised by vertical and lateral facies heterogeneity whereby sand-prone packages are draped and partitioned by mud-prone deposits of variable thickness and continuity in response to temporal and spatial variation in depositional processes. In contrast to sand-dominated point-bar elements, counter point-bar elements typically comprise mud-dominated lithofacies whereby distinctive concave scroll patterns are formed by downstream meander translation, notably in systems space constrained by incised valleys, local tectonics, or erosion-resistant mud-filled abandoned channel elements (Ghinassi et al., 2016; Smith et al., 2009).

(a) expansion

(b) expansion & rotation

(c) translation

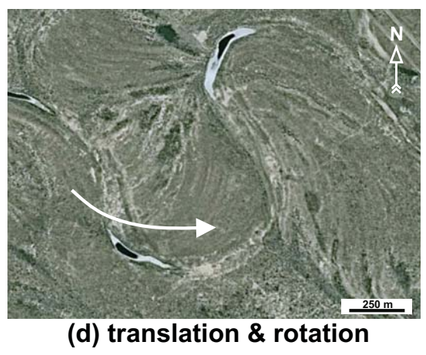

(d) translation & rotation

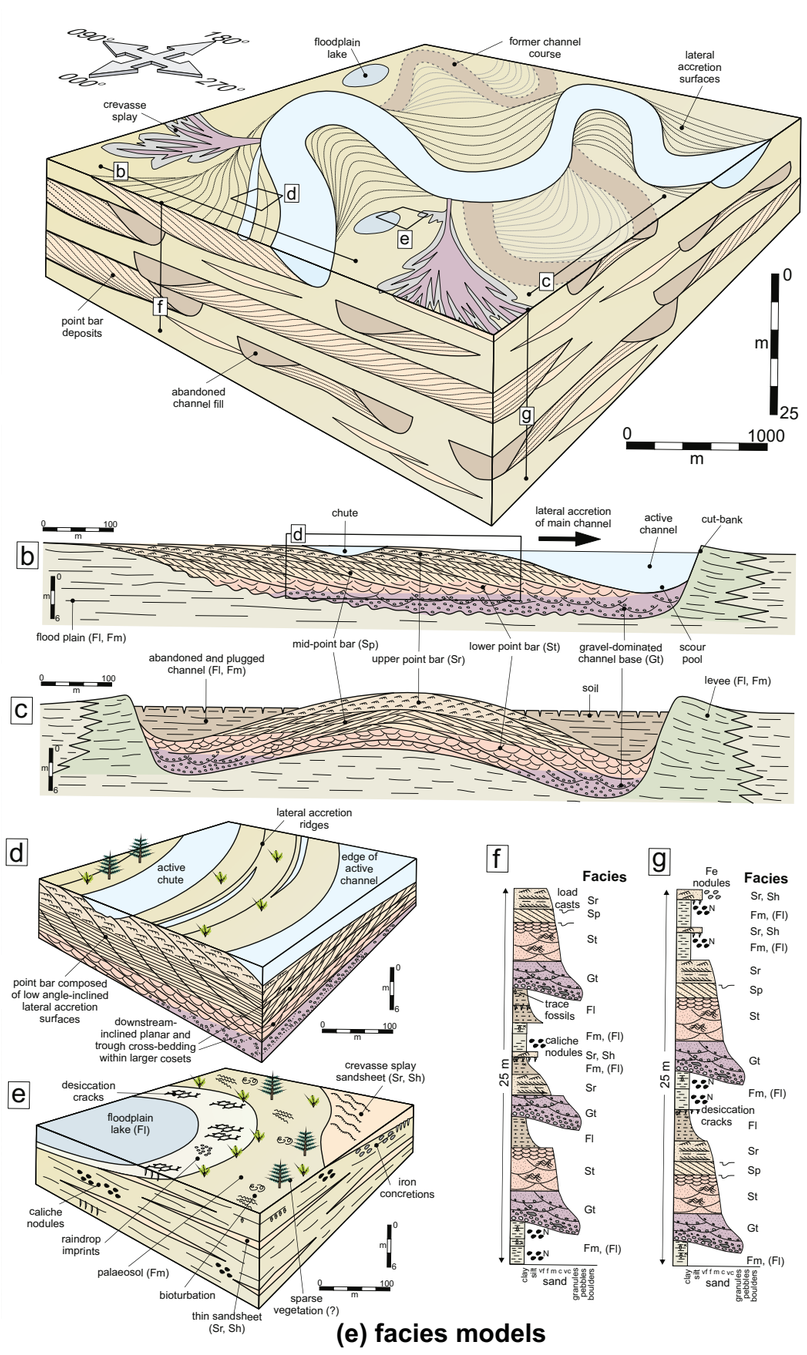

(e) facies models

Fig. 1. Basic forms of meander-bend transformations: (a) expansion, Songhua River, China; (b) expansion and rotation, Mississippi River, USA; (c) translation, Rio Negro, Argentina; (d) translation and rotation, Rio Negro, Argentina. Arrows show migration directions of scroll bars. (e) Traditional meandring river facies models built from observation of facies and their spatial distribution from limited number of case-studies (Ghazi & Mountney, 2009).

Forward Stratigraphic Modelling Algorithm

The modelling workflow uses a combined geometric-based, process, and stochastic approaches to reconstruct the complex spatio-temporal evolution of a variety of meandering river behaviours and to predict variations in 3D geometry and lithofacies distribution of sand- and mud-prone packages of point bars under different conditions of channel migration. The modelling algorithm is based on key parameter controls, such as the meander-bend transformation style, degree of sinuosity, distance from meander apex, and the locations of the inflection points of meanders and their change in position over time.

Morphological Evolution of Point-bar Elements in Plan View

(a) Kinabatangan River, Malaysia

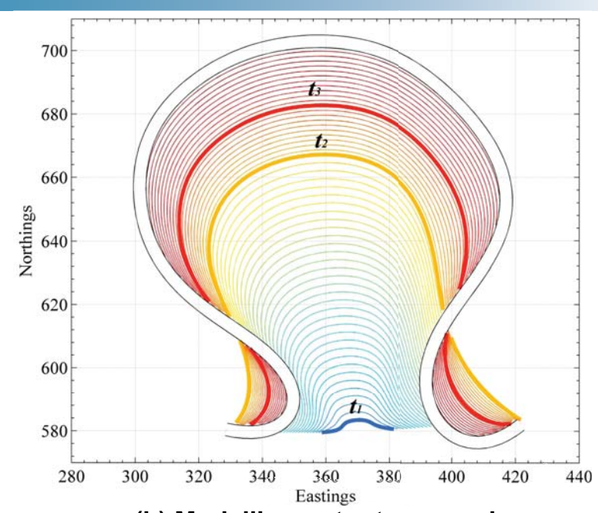

(b) Modelling output: expansion

Fig. 2. Modelling the evolution of point bars in plan view. The temporal locations at t_1, t_2, and t_3 are shown in bold lines. A jet colour (dark blue to dark red) scheme is used to differentiate meander positions at different times. The spatial dimensions here are arbitrary, but the modelling results can be readily scaled to physical units based on data from field measurements or remote sensing. The shape of the modelled point bar is comparable with that of point-bar elements commonly found preserved in the ancient rock record.

Cross-sectional Complexity and Lithofacies of Point-bar Architecture

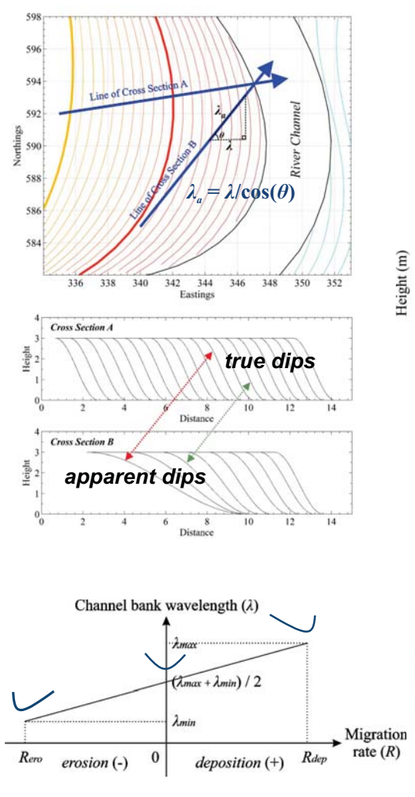

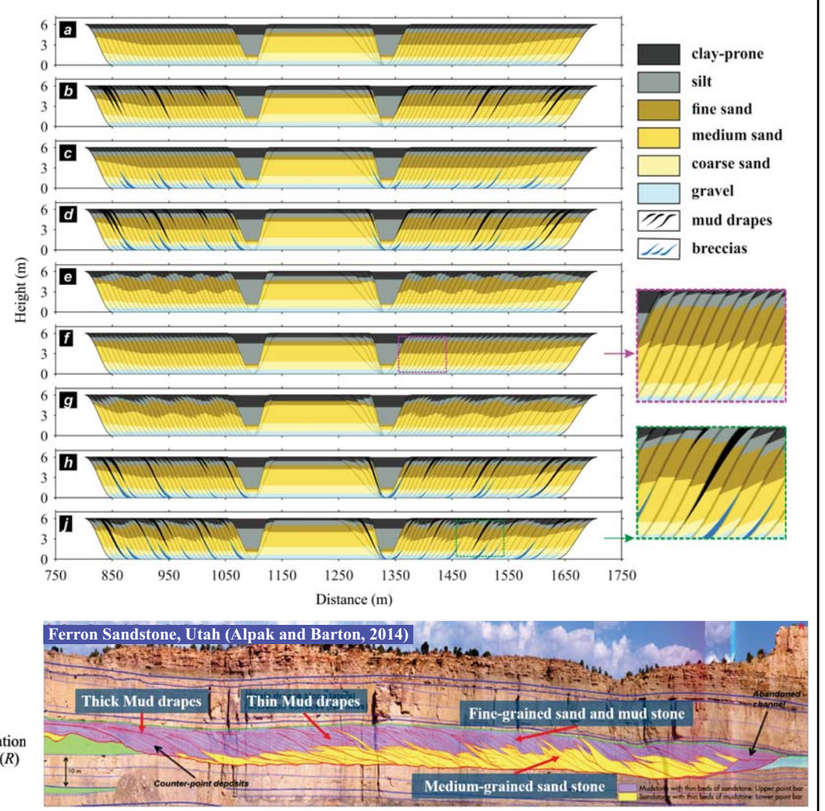

Fig. 3. Illustration of the method for calculating the wavelength of accretion surfaces, which in its simplest form, is modelled as sine-curve. The channel-bank wavelength is determined by the migration rate and morphology change caused by erosion or deposition.

Fig. 4. Examples of modelled cross sections with different lithological characteristics: (a) basic lithological arrangement with fining-upward trend; (b d h) cross sections with mud drapes; (c d h j) cross sections with basal breccias; (e g j) cross sections with randomised facies components; and (f g h j) cross sections with inter-digitated facies. Note vertical exaggeration. Comparison of modelled cross-section examples (j) with an outcrop of Ferron Sandstone in Utah, USA. The modelled cross sections can mimic outcrops seen in real-world.

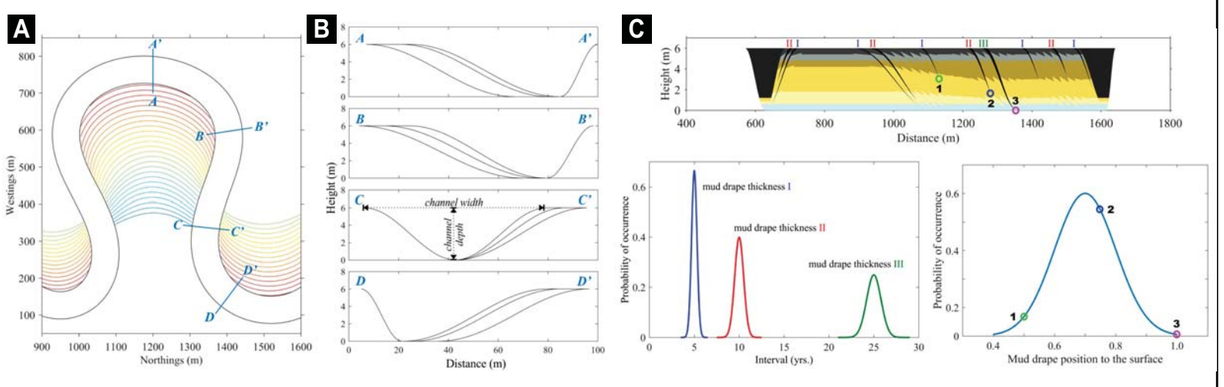

Fig. 5. Algorithm for modelling the shape of channel banks. (A) Plan-view locations of representative cross sections. (B) Channel-bank profiles of representative cross sections. (C) Examples of modelling multiple-scale mud drapes with three different thicknesses (I, II and III) that are controlled by their respective probability curves of occurrence. The vertical position of the point to which mud drapes extend down the bar front are also modelled using a Gaussian distribution curve specified by users; three examples are shown in circles.

Applications of PB-SAND

PB-SAND is a numerical model for the forward modelling of the development of stratigraphic architectures and internal lithofacies distributions associated with fluvial point-bar elements, and similar elements present in fluvial and tidally influenced fluvial systems (Yan et al., 2017). PB-SAND is coded in Matlab with a user interface programmed in C#. It is designed as a tool for sedimentary research and finds specific application in aiding the development of improved reservoir modelling workflows, whereby PB-SAND can be used to generate training images for use in MPS modelling workflows, and numerical output can be used in object-based modelling workflows using industry standard software such as Schlumberger Petrel. The model can be applied to reconstruct the complex spatio-temporal evolution of a variety of meandering river behaviours and to understand potential evolutionary trajectories and sedimentary structures of both ancient and modern fluvial meandering systems. The model (i) serves as a useful tool to improve our understanding of the origin of stratigraphic complexity and heterogeneity in fluvial depositional systems at a variety of different spatial scales, and (ii) is directly applicable to subsurface hydrocarbon reservoir and groundwater aquifer appraisal.

Predict Fluvial Point-bar Architecture and Facies Heterogeneity

Humid coastal-plain systems

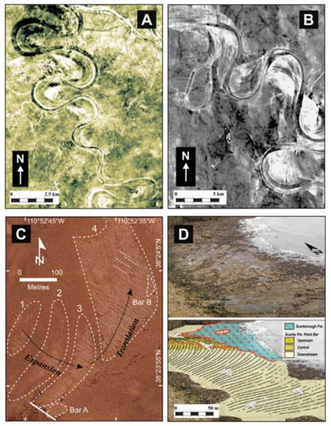

VS

Dryland fluvial-fan systems

Fig. 6. Examples of fluvial point-bar elements in humid coastal-plain systems. (A) Point-bar elements in the Upper Arang Formation, Middle Miocene, West Natuna Basin, off-shore Indonesia, imaged in high-resolution 3D seismic data (adapted from Maynard & Murray, 2003). (B) Point-bar elements in the Tertiary Pattani rift basin, Gulf of Thailand, imaged in high-resolution 3D seismic data (adapted from Reijenstein et al., 2011). (C) An ancient point-bar element in the Ferron Sandstone of Cretaceous Notom Delta, Utah, USA; note the channel migration directions indicated on the satellite image (adapted from Wu et al., 2015). (D) Point bar elements in the Jurassic Scalby Formation, UK; note the interpretations of different parts of point-bar elements (adapted from Ghinassi & Ielpi, 2015).

Fig. 7. Examples of fluvial point-bar elements in interpreted dryland fluvial-fan systems. (A) Meander-bend scroll bars in the Upper Triassic Chinle Formation at Petrified Forest National Park, Arizona, USA (adapted from Trendell et al., 2013). (B) Reiersvlei meanders (32° 02′ S, 22° 03′ E) in the Permian Beaufort Group of the Southwestern Karoo, South Africa (image from Google Earth; cf. Smith, 1987). (C) Point-bar elements (38° 24′ N, 111° 01′ W) in the Upper Jurassic Morrison Formation, Utah, USA (image from Google Earth; cf. Hartley et al., 2015). (D) Point-bar elements (39° 10′ N, 110° 52′ W) in the Upper Jurassic Morrison Formation, Utah, USA (image from Google Earth; cf. Hartley et al., 2015). (E) Outcrop of a point-bar sandstone body with well-preserved clay plug and lateral-accretion surfaces from the Miocene Huesca fluvial fan, Ebro Basin, Spain (adapted from Donselaar & Overeem, 2008).

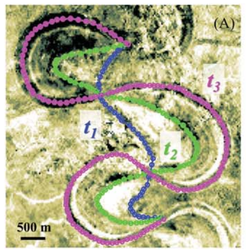

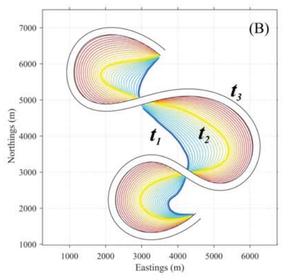

Fig. 8. Modelling morphology evolution of point bars. (A) Blue, green, and pink circles represent input coordinates of channel trajectories at t_1, t_2, and t_3 respectively, which are digitised from the seismic image in the Upper Arange Formation of Middle Miocene, West Natuna Basin, off-shore Indonesia (Maynard and Murray, 2003). (B) Morphology of point bars modelled by PB-SAND with highlighted channel trajectories at t_1, t_2, and t_3.

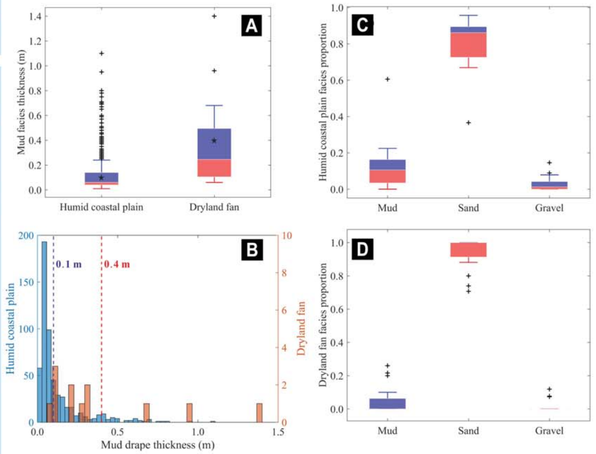

Fig. 9. Input parameters from real-world case examples extracted from FAKTS database (Colombera et al., 2013). (A) and (B) show the distribution of mud-drape thickness in humid coastal plain and dryland fan systems. (C) and (D) show the proportions of mud, sand, and gravel facies in point-bar elements of humid coastal plain and dryland fan systems, respectively. See details in Yan et al. (2018).

Predict Fluvial Point-bar Architecture and Facies Heterogeneity

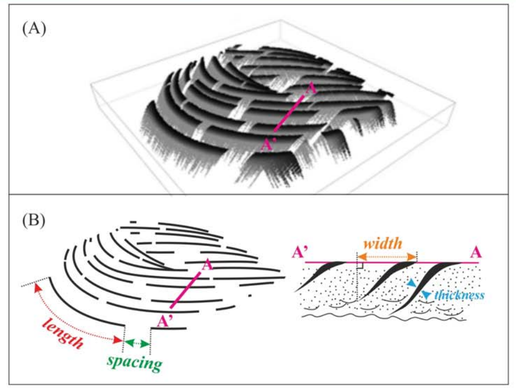

Fig. 10. Examples of the length, the lateral spacing, and the width (the projected extent in horizontal surface) of mud drapes shown in a 3D modelling output of a modelled point bar generated using PB-SAND.

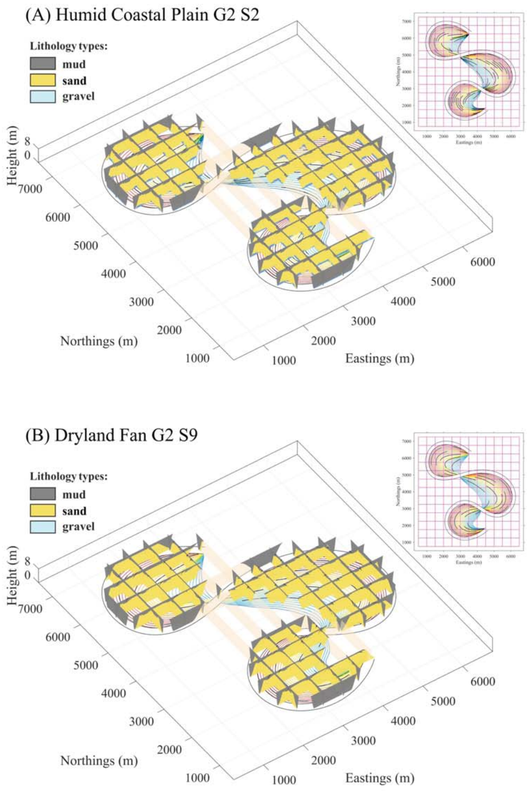

Fig. 11. Three-dimensional fence diagrams of representative simulations in (A) humid coastal-plain systems and (B) dryland fluvial-fan systems.

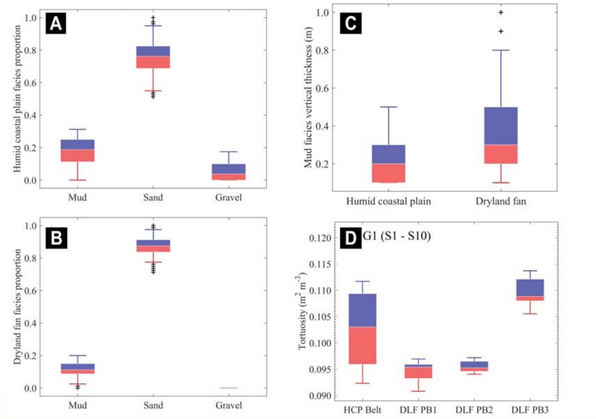

Fig. 12. Statistical outputs from modelled point-bar elements. Lithological facies proportions from PB-SAND modelling outputs in (A) humid coastal-plain systems vs. (B) dryland fluvial-fan systems; which are closely comparable to their counterparts in the input data (Fig. 9). (C) The vertical thickness of mud drapes sampled from simulation outputs. (D) Tortuosity of connected sand geo-bodies. A single connected deposit is recognised in the meander belt modelled using the humid coastal-plain analogues (HCP Belt), whereas three isolated point-bar elements (DLF PB1, DLF PB2, and DLF PB3) are modelled using the dryland fluvial-fan analogues.

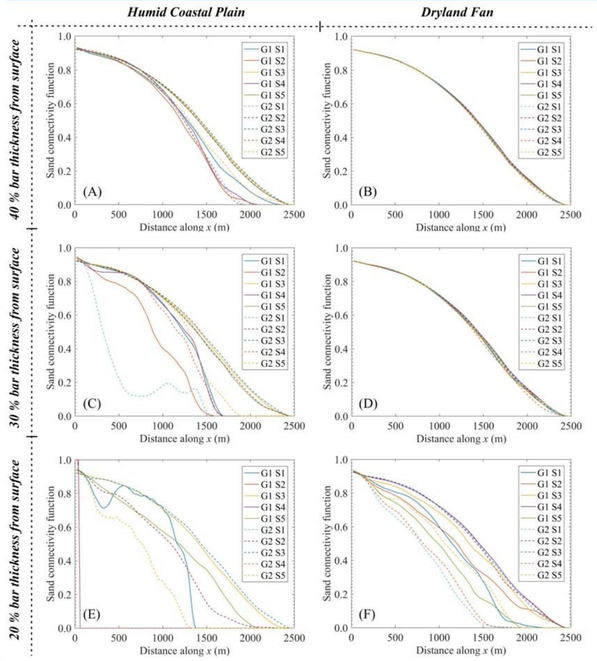

Fig. 13. Changes of the connectivity functions of sand along x (across channel belt) direction in simulations.

Improve Geocellular Modelling of Fluvial Meander-belt Reservoirs

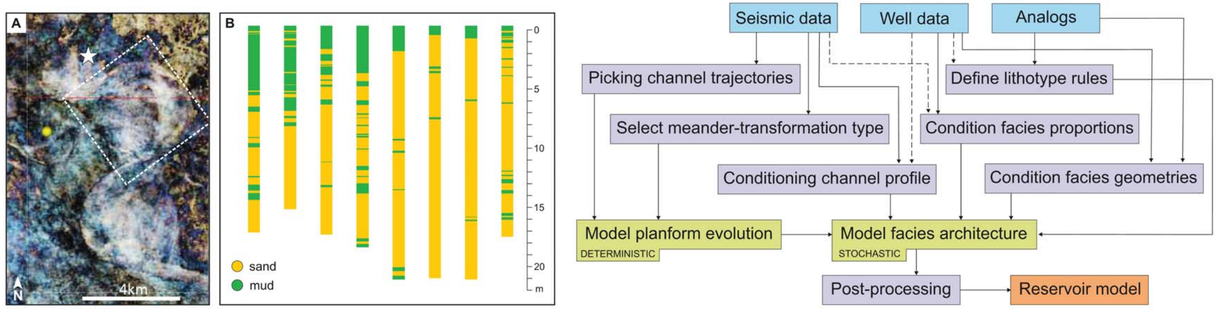

Fig. 14. (A) Seismic time slice through the meander-belt deposits. (B) Facies logs from eight of the wells drilled in the northern point-bar body; only the interval interpreted as point-bar deposits is represented. (C) Flow chart of workflows for the creation of static models for large point-bar reservoirs using PB-SAND; boxes represent inputs (blue), operations (purple), and outputs (green). Dashed lines indicate additional routes by which some observations could be used to constrain modeling operations. See details in Colombera et al. (2018).

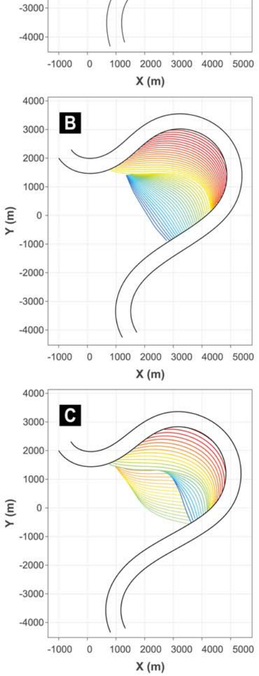

Fig. 15. Plan views of three scenarios of plan form evolution modelled for the central point-bar body, respectively assuming simple meander expansion (A), expansion and rotation (B), and translation followed by expansion (C). Coloured lines represent point-bar accretion surfaces obtained by interpolation of channel trajectories at significant times. Black lines represent the margins of the genetically related channel fill associated with the youngest channel trajectory used to condition the models. The three channel centre-line used to condition the planform models are represented by: a blue curve (time 1), a yellow curve (time 2), and the centre line of the channel fill (time 3). Two stages of evolution, each including three time steps, were modelled for the scenario in part C.

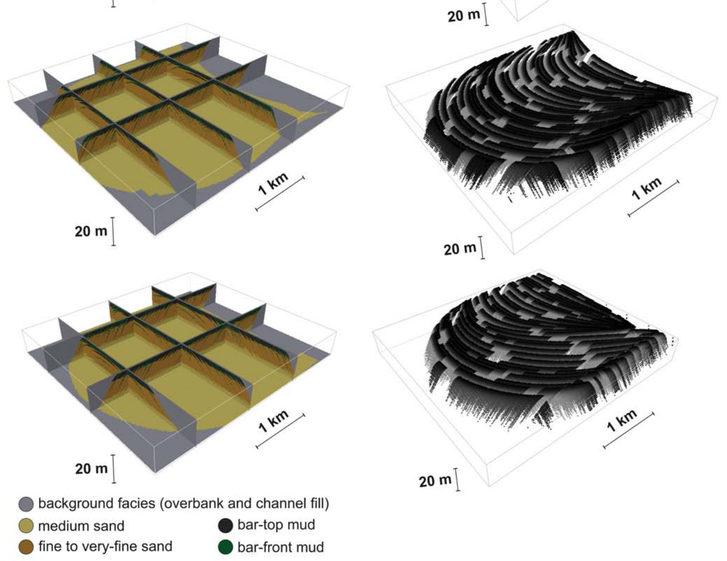

Fig. 16. Geocellular models (upscaled grids) for the central point-bar body built using PB-SAND. Fence diagrams of the grids are shown on the left-hand side, coded by facies type. Shaded 3D views of the modeled mud drapes in each simulation are shown on the right-hand side.

Improve Geocellular Modelling of Fluvial Meander-belt Reservoirs

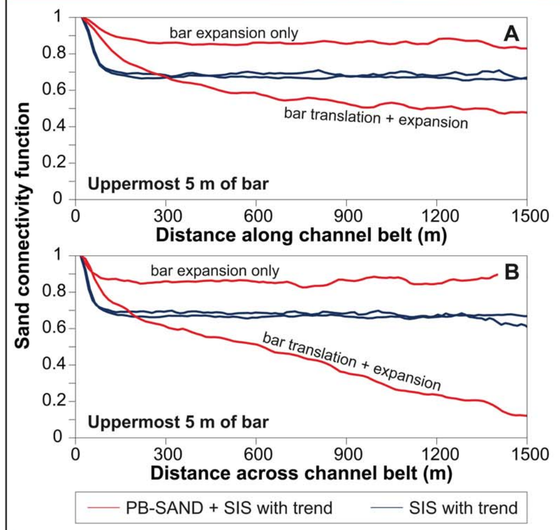

Fig. 17. Comparison between the two models for the northern point bar created combining PB-SAND with SIS (red), and two corresponding SIS models that were not conditioned on regions generated with PB-SAND (blue). The models that incorporate accretion geometries generated using PB-SAND are characterised by significant difference in connectivity functions, highlighting the importance of accounting for styles of meander growth when modelling facies distributions.

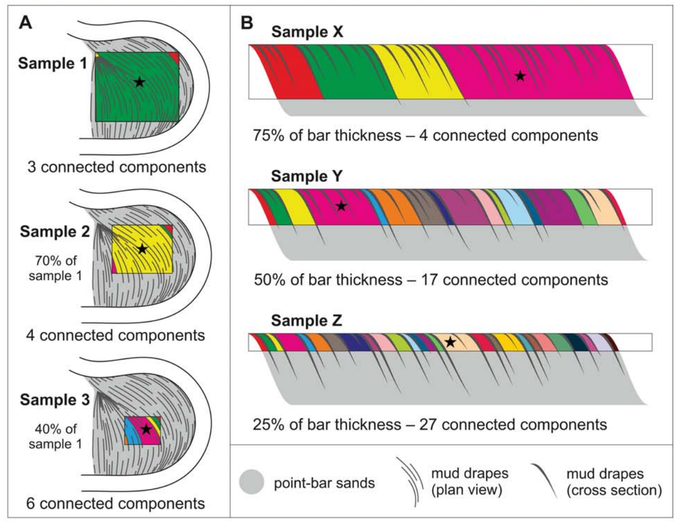

Fig. 18. Idealised examples that illustrate the effect of sample size on the number and size of connected components made of point-bar sands that are compartmentalized by mud drapes, in both plan view (A) and cross sections (B). In each sample (black frames), different connected components of point-bar sands are represented as variably coloured sectors. The largest connected components in each sample are denoted by stars.

References

Alexander, J., and M. R. Leeder, 1987, Active tectonic control on alluvial architecture, in F. G. Ethridge, R. M. Flores, and M. D. Harvey, eds., Recent Developments in Fluvial Sedimentology, SEPM Special Publication 39, p. 243-252.

Colombera, L., Mountney, N.P., McCaffrey, W.D., 2013. A quantitative approach to fluvial facies models: Methods and example results. Sedimentology, 60, 1526-1558.

Colombera, L., Yan, N., McCormick-Cox, T., Mountney, N.P., 2018. Seismic-driven geocellular modeling of fluvial meander-belt reservoirs using a rule-based method. Marine and Petroleum Geology.

Donselaar, M.E., Overeem, I., 2008. Connectivity of fluvial point-bar deposits: An example from the Miocene Huesca fluvial fan, Ebro Basin, Spain. AAPG Bulletin, 92(9), 1109-1129.

Ghazi, S., Mountney, N.P., 2009. Facies and architectural element analysis of a meandering fluvial succession: The Permian Warchha Sandstone, Salt Range, Pakistan. Sedimentary Geology, 221(1-4), 99-126.

Ghinassi, M., Ielpi, A., 2015. Stratal Architecture and Morphodynamics of Downstream-Migrating Fluvial Point Bars (Jurassic Scalby Formation, U.K.). Journal of Sedimentary Research, 85(9), 1123-1137.

Ghinassi, M., Ielpi, A., Aldinucci, M., Fustic, M., 2016. Downstream-migrating fluvial point bars in the rock record. Sedimentary Geology, 334, 66-96.

Hartley, A.J., Owen, A., Swan, A., Weissmann, G.S., Holzweber, B.I., Howell, J., Nichols, G., Scuderi, L., 2015. Recognition and importance of amalgamated sandy meander belts in the continental rock record. Geology, 43(8), 679-682.

Maynard, K., Murray, I., 2003. One Million Years from the Upper Arang Formation, West Natuna Basin, Implications for Reservoir Distribution and Facies Variation in Fluvial Deltaic Deposits.

Reijenstein, H.M., Posamentier, H.W., Bhattacharya, J.P., 2011. Seismic geomorphology and high-resolution seismic stratigraphy of inner-shelf fluvial, estuarine, deltaic, and marine sequences, Gulf of Thailand. AAPG bulletin, 95(11), 1959-1990.

Smith, D.G., Hubbard, S.M., Leckie, D.A., Fustic, M., 2009. Counter point bar deposits: lithofacies and reservoir significance in the meandering modern Peace River and ancient McMurray Formation, Alberta, Canada. Sedimentology, 56, 1655-1669.

Smith, R.M.H., 1987. Morphology and depositional history of exhumed Permian point bars in the southwestern Karoo, South Africa. Journal of Sedimentary Research, 57(1), 19-29.

Smith, D.G., Hubbard, S.M., Lavigne, J.R., Leckie, D.A., Fustic, M., 2011. Stratigraphy of counter-point-bar and eddy-accretion deposits in low-energy meander belts of the Peace-Athabasca Delta, Northeast Alberta, Canada. In: S.K. Davidson, S. Leleu, C.P. North (Eds.), From River to Rock Record: The Preservation of Fluvial Sediments and Their Subsequent Interpretation. Society for Sedimentary Geology Special Publication. S E P M - Soc Sedimentary Geology, Tulsa, pp. 143-152.

Trendell, A.M., Atchley, S.C., Nordt, L.C., 2013. Facies analysis of a probable large-fluvial-fan depositional system: the Upper Triassic Chinle Formation at Petrified Forest National Park, Arizona, USA. Journal of Sedimentary Research, 83(10), 873-895.

Wu, C., Bhattacharya, J.P., Ullah, M.S., 2015. Paleohydrology and 3D facies architecture of ancient point bars, Ferron Sandstone, Notom Delta, south-central Utah, USA. Journal of Sedimentary Research, 85(4), 399-418.

Yan, N., Mountney, N.P., Colombera, L., Dorrell, R.M., 2017. A 3D forward stratigraphic model of fluvial meander-bend evolution for prediction of point-bar lithofacies architecture. Computers & Geosciences, 105, 65-80.

Yan, N., Mountney, N.P., Colombera, L., Dorrell, R.M., 2018. Fluvial point-bar architecture and facies heterogeneity, and their influence on intra-bar static connectivity in humid coastal-plain and dryland fan systems. Special Publications of the International Association of Sedimentologists, 48.

Integration of Numerical Modelling Approach

Literature

Field Studies

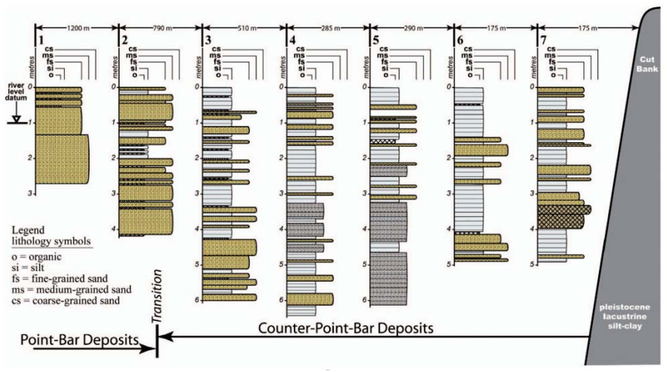

Peace River, Alberta (Smith et al., 2011)

Fig. 19. Examples of data from literature and field studies.

Database (FAKTS)

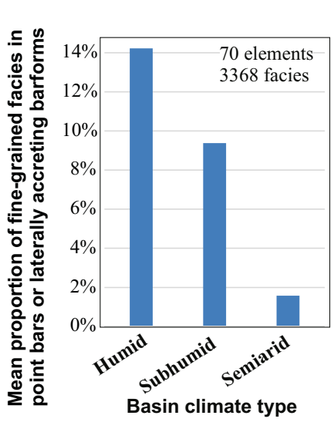

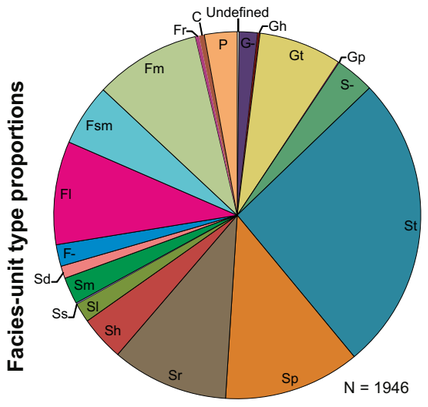

(Colombera et al., 2013)

1D QUANTITATIVE FACIES MODEL FOR SANDY MEANDERING SYSTEMS

- G: gravel; S: sand; F: fines;
- P: pedogenic carbonate;
- C: coal or organic mud;
- h: horizontally bedded sand (Sh) or crudely bedded gravel (Gh);
- t: trough cross-bedded;
- p: planar cross-bedded;
- l: low-angle cross-bedded sand (Sl) or laminated mud (Fl);
- r: ripple cross-laminated sand (Sr) or root-bed fines (Fr);
- s: scour fill;
- m: massive sand (Sm) or massive mud (Fm);
- d: soft-sediment deformation;
- sm: silt and mud.

Numerical Modelling

Parameters of Scalby Formation

		Mean	Min	Max	Std.
	bar thickness (m)	6			
	channel width (m)	74			
mud drape	thickness (m)	0.20	0.06	0.66	0.18
	length along accretion surfaces (m)	7.80	1.60	19.00	4.56
	spacing (m)	5.74	1.90	10.20	2.56
	position (to the top) (m)	1.35	0.28	3.30	0.79
	position (to the top)	23 %	5 %	55 %	13 %
facies	mud-prone	11 %			
	very fine sand	7 %			
	fine sand	37 %			
	medium sand	45 %			

Frequency Distribution Curves

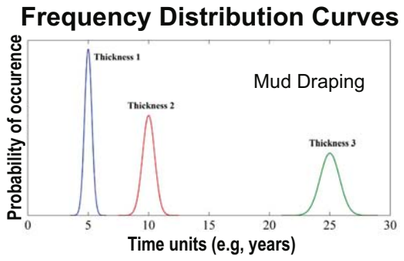

Model Components:

- Morphological evolution
- Vertical cross sections
- Stacking patterns

3D Architecture

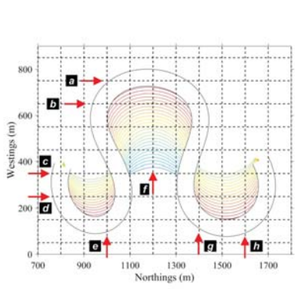

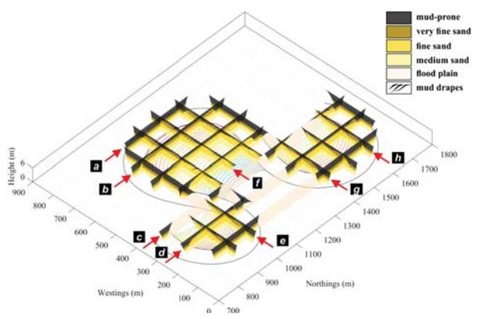

Model Outupts:

- High resolution morphology
- Facies distribution
- Bounding surfaces
- Probability of possible scenarios
- Sensitivity of major environmental controls
- Prediction of 3D architecture
- 2D and 3D figures

Reservoir Software

Grid-based models

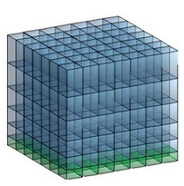

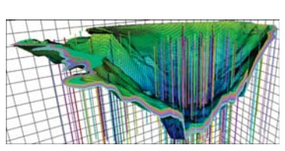

Schlumberger Petrel™

Baker Hughes JewelSuite™

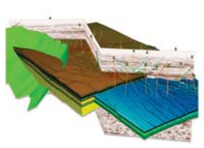

Landmark DecisionSpace™

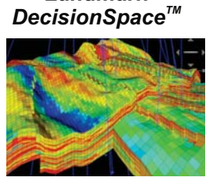

PB-SAND Summary

Input Parameters of PB-SAND

SINGLE POINT BAR

- point bar transformation style
- coordinates of bar positions at three key times (x, y)
- migration rates (m yr^{-1}) or bar numbers (# m^{-1}) between key times

CHANNEL ASYMMETRY AND SHAPE OF INCLINED ACCRETION SURFACES

- river width (m)
- bar depth (m)
- dip angle (º)
- maximum deposition rate of inner bank (m yr^{-1})

LOCATION OF CROSS SECTIONS

- cross section area
  - width (m)
  - length (m)

FACIES ASSOCIATIONS

- point bar transformation style
- facies types
- proportions of different facies at representative point-bar locations
  - early stage expansional point bar
  - mature stage and high sinuosity expansional point bar

SHAPE OF FACIES BOUNDING SURFACES

- inclination for each bounding surface
  - minimum and maximum degree of inclination (º)
  - minimum and maximum years of a cycle (m)
  - shape factor of Gaussian distribution curve for cycling years
- disorder & randomness level for each bounding surface

MULTIPLE POINT BARS

- percentage of different bar transformation styles
- orientation distribution curve (º, unimodal or bimodal)
- size distribution curve
- point bar longevity control (time or cut-off)
- point bar density distribution in a channel belt

MUD DRAPES

- probability distribution curves of 1-3 different levels of mud drapes
  - thickness (m)
  - minimum occurrence interval (yrs)
  - maximum occurrence interval (yrs)
  - shape factor of Gaussian distribution curve for interval
- position of mud drapes on bar front
  - upper boundary of mud drape front relative to bar depth
  - lower boundary of mud drape front relative to bar depth
  - shape factor of Gaussian distribution curve for position
- continuity of mud drapes in cross sections
  - maximum numbers (1-3) of gaps within a mud

CONGLOMERATES OR BRECCIAS

- probability distribution curves of 1-3 different levels of conglomerates or breccias
  - thickness (m)
  - minimum occurrence interval (yrs)
  - maximum occurrence interval (yrs)
  - shape factor of Gaussian distribution curve for interval

Outputs of PB-SAND

- high-resolution plan-view morphology
- facies distribution in 3D
- bounding surface geometries (2nd order)
- mud drapes at different scales (3rd order)
- multiple point-bar elements in a meander belt
- stacking patterns and connectivity change caused by different subsidence rates and avulsion rates
- sensitivity of parameter controls
- cross sections training images for MPS
- 3D fence diagrams

GUI of PB-SAND

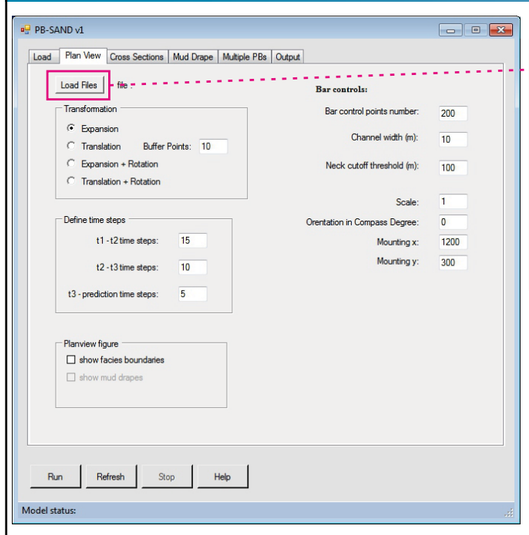

Library of point-bar elements with scroll bar positions

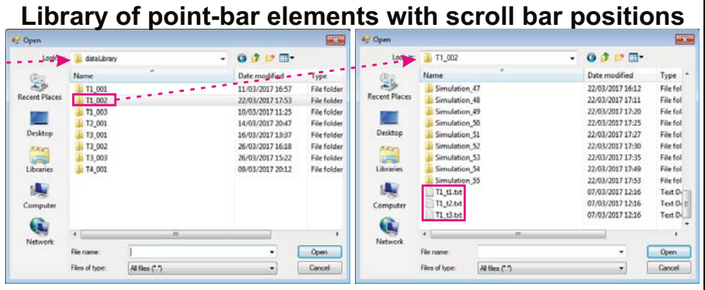

Fig. 20. Demonstration of PB-SAND input file structure. The library of point-bar examples are organised in their respective folders. Three text files define the coordinates of scroll-bar locations at three key times. Output files are automatically generated in each simulation run.

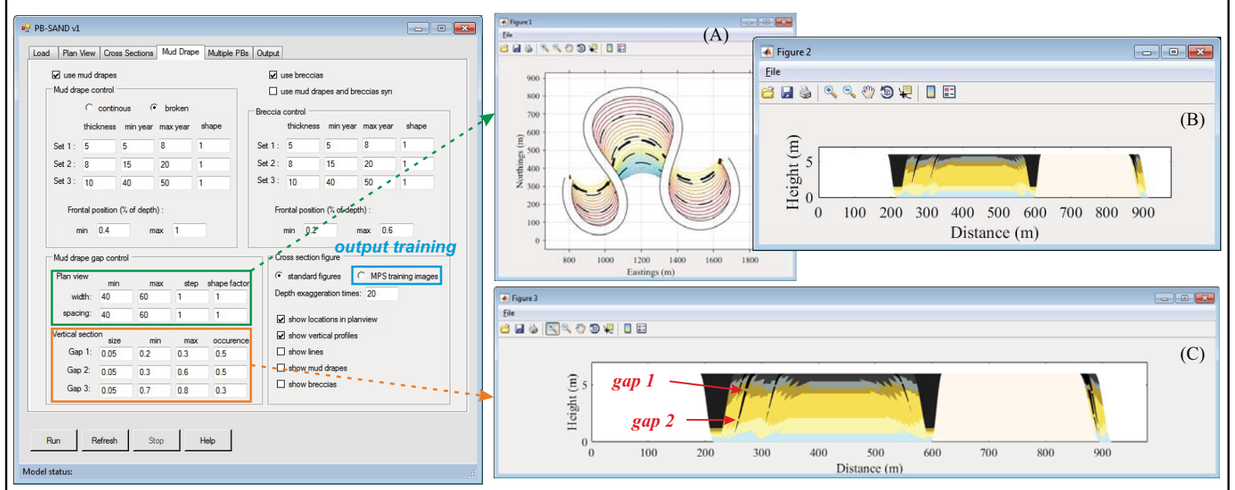

Fig. 21. Demonstration on modelling controls used to define the distribution of mud drapes. (A) An example of discontinuous mud drapes in plan view. (B) An example of continuous mud drapes in vertical cross section. (C) An example of discontinuous mud drapes in vertical cross section. The sizes and locations of discontinuities in the mud drapes can be controlled by their respective Gaussian distribution curves.

AkerBP
AREVA
bhpbilliton
CAIRN
WE FUEL AMAZING
ConocoPhillips
MURPHY OIL CORPORATION
NERC SCIENCE OF THE ENVIRONMENT
CNOOC nexen A CNOOC LIMITED COMPANY
pds petrotechnical
ارامكو السعودية Saudi Aramco
TULLOW Plc
woodside
YPF